Article:
Wilczynski, F and Hughes, DW orcid.org/0000-0002-8004-8631 (2019) Stability of two-layer miscible convection. Physical Review Fluids, 4 (10). 103502. ISSN 2469-990X

https://doi.org/10.1103/PhysRevFluids.4.103502

Stability of two-layer miscible convection

F. Wilczynski[1,*] and D. W. Hughes[2]

[1] *EPSRC CDT in Fluid Dynamics, University of Leeds, Leeds LS2 9JT, United Kingdom*
[2] *School of Mathematics, University of Leeds, Leeds LS2 9JT, United Kingdom*

(Dated: August 21, 2019)

The dynamics at the edge of fusion confinement devices involves the motion of plasma across two regions — the core and the scrape off layer — that may have very different properties. Motivated by this problem, and exploiting the analogy between the equations governing plasma interchange dynamics and those of classical Rayleigh-Bénard convection, we consider the linear stability of two-dimensional, two-layer miscible convection. We focus specifically on the influence of three particular parameters: the ratio of the viscosities in the two layers, the ratio of the thermal diffusivities, and the ratio of the depths of the two layers. The key result is that, depending on the parameters of the problem, the most unstable mode can take one of three quite distinct forms: *whole layer* solutions, in which the eigenfunctions of the stream function and temperature extend over both layers of fluid; *localized* solutions, with the velocity cells or the temperature perturbation (or both) confined to just one of the layers; and *segregated* solutions, in which the fluid motion and temperature perturbation are confined to different fluid layers.

* scfw@leeds.ac.uk

I. INTRODUCTION

Rayleigh–Bénard convection is a classical problem in fluid dynamics, describing the instability of a fluid layer heated from below. Thermal convection has applications in a wide range of phenomena in geophysics, astrophysics, meteorology, oceanography and engineering. It played a crucial role in the development of stability theory in hydrodynamics [1], and the rapidly expanding literature on applications of convection indicates a continuing demand for an improved understanding of its properties.

In this paper we consider a two-layer extension of the classical Rayleigh–Bénard problem. Two-layer convection consists of two horizontal layers of fluid, one above the other, heated from below. The two layers can have different depths, are characterized by different thermal and mechanical properties (i.e. density, viscosity, thermal diffusivity, thermal expansion coefficient etc.), and are separated by a thin interface, which couples the behavior in the two layers through mechanical and thermal continuity conditions. Layered convection systems are frequently found in planetary and astrophysical fluid dynamics. Studies of two-layer convection were originally motivated by its suggested occurrence in the Earth's mantle [2, 3]. Stellar interiors are commonly segregated into layers with distinct characteristics, for example with a convectively unstable layer sandwiched between stable layers [4]. Multiple-layer convection problems also arise in industrial applications of molten material, particularly in the area of crystal growth [5].

The problem of convection in superposed layers has attracted considerable attention because of its interesting theoretical aspects. The ostensibly simple addition of a second convecting layer engenders a rich variety of qualitatively new phenomena, such as competition between instabilities in the separate layers, oscillatory behavior at the onset of convection, deformations of the interface, and interfacial surface tension driven modes. Owing to the large number of potentially relevant parameters, the wealth of possible behavior is impressive. Whereas convection in a single layer of Boussinesq fluid is governed by just two dimensionless parameters, the Rayleigh and the Prandtl number, of which the latter does not enter into the stability criterion, up to ten parameters may be important for the two-layer problem. Parameters such as layer height ratios, various fluid property ratios and surface tension gradient all diversely affect the onset of convection in the layers, resulting in a variety of distinct convection modes. There have been a number of papers dedicated to exploration of some particular subspace of the parameter space, with the goal of extracting conditions for the occurrence of different convection modes [e.g. 6, 7]. Certain aspects of the nonlinear problem, involving the interaction of modes of different spatial extent, have been addressed in Ref. [8].

In this paper, we study a simple two-layer convection problem in order to gain insight into a plasma instability occurring at the edge of magnetic confinement fusion devices [9]. Although in the following sections we shall consider a purely hydrodynamic problem, it is necessary briefly to sketch out some relevant background in order to elucidate the motivation for this study. Readers more interested in the analysis of the mathematical problem may pass directly to Section II.

Magnetic confinement fusion is an approach to generating thermonuclear fusion power that uses magnetic fields to confine hot fusion fuel in the form of a plasma. The magnetic confinement device that shows most promise in terms of producing viable fusion power is the tokamak. A modern tokamak consists of a toroidally shaped vacuum vessel, around which magnetic coils are wound; these coils generate magnetic field lines that wind helically around the torus and form nested closed surfaces — *flux surfaces* — on which the flux of poloidal magnetic field is constant. Perfect confinement would be achieved if the plasma remained on these surfaces indefinitely. In reality, various plasma phenomena cause instabilities and confinement issues, resulting in a plasma drift, from surface to surface, despite the presence of the confining magnetic field. This drift, if uninterrupted, will eventually result in plasma impacting on the walls of the tokamak chamber, potentially damaging the components of the device. To reduce the plasma-surface interaction, modern tokamaks utilize a configuration that produces a *diverted* plasma. The poloidal magnetic field is shaped to create distinct regions of plasma inside the tokamak — the core and the scrape-off layer (SOL) — and thus to divert the escaping plasma into a specifically designed structure known as the divertor (see Fig. 1). The two regions are separated by a magnetic separatrix and are topologically distinct. In the core, the magnetic field lines close back upon themselves and do not come in contact with material surfaces. By contrast, the scrape-off layer is the region of open field lines situated between the separatrix and the vessel wall; the magnetic field lines are open in the sense that they penetrate a solid surface. The topological distinction between the core and SOL regions has profound consequences on plasma dynamics in the direction parallel to the magnetic field. Since every field line in the SOL is connected to a material surface, the SOL plasma is always subject to parallel losses of particles and energy.

The classical picture of edge plasma dynamics assumes that parallel transport processes are dominant in the SOL, whereas radial transport is weak and diffusive. As such, a plasma particle that drifts out of the core into the SOL is transported along the magnetic field and deposited onto the target surfaces before it reaches the chamber wall. However, contrary to this assumption, it has been widely observed that turbulence in the SOL is characterized by intermittent ejections of dense coherent plasma structures, often called filaments or blobs [10, 11]; these filaments are responsible for transporting plasma and energy from the well-confined region towards the material surfaces. As discussed above, this is problematic, since plasma-wall interaction can potentially cause significant erosion and hence

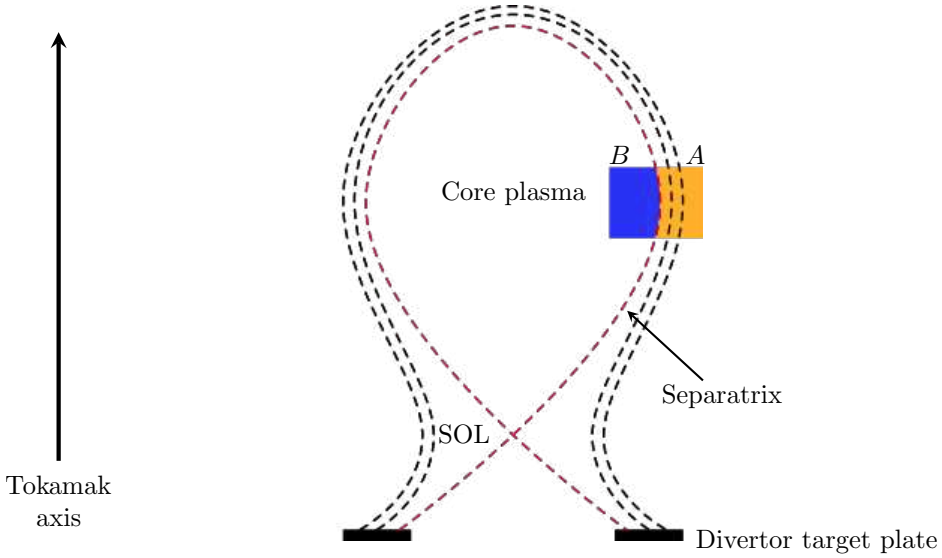

FIG. 1: Sketch of the poloidal cross section of a diverted tokamak plasma.

shorten the lifetime of the machine. Furthermore, large fluxes of plasma impinging on material walls can cause surface particles to become liberated from the material and enter the core of the plasma as impurities. Once there, they radiate energy, thus reducing the temperature of the plasma and the performance of the tokamak. A full understanding of filament dynamics is therefore essential for the successful operation of future fusion experiments and reactors.

Over the last two decades, significant experimental and theoretical work has been devoted to understanding the fundamental mechanisms governing the dynamics in the scrape-off layer of magnetic fusion devices. It is now widely recognized that turbulent motions in the SOL are dominated by interchange dynamics, supplemented by parallel losses to the plasma-solid interface. SOL interchange models have been studied extensively, both theoretically and numerically, and have provided useful insight into the dynamics of SOL plasma. The simplest, two-dimensional models consider the dynamics of plasma in the plane perpendicular to the magnetic field, in the region of plasma edge located at the outermost part of the torus (the solid shaded region A in Fig. 1), under the so-called slab approximation, whereby the geometry is simplified to a local slab with a uniform magnetic field, with the effects of magnetic curvature and magnetic gradients represented through an effective gravitational acceleration acting in the radial direction. The dynamics of plasma parallel to the magnetic field can be modelled by the implementation of a suitable closure for the current along the field lines. The model equations are derived from the Braginskii fluid equations [12], and, at the very basic level, consist of evolution equations for density conservation and plasma vorticity (which determines the plasma potential).

Interchange instability at the plasma edge arises from pressure gradients in a plasma constrained by an inhomogeneous magnetic field. In the simple picture in Fig. 1, plasma pressure on the inner (left) boundary of the shaded region is significantly higher than that on the outer (right) boundary. The curvature and gradient of the magnetic field result in an effective gravitational force acting radially towards the axis of the tokamak (i.e. to the left here). Thus, the equilibrium pressure gradient points in the same direction as the effective gravitational acceleration, thereby leading to unstable stratification. The plasma is thus susceptible to interchange instability in which high pressure plasma is interchanged with neighboring lower pressure regions in an overturning motion. This mechanism is analogous to that of Rayleigh-Bénard convection, in which overturning motions arise owing to the presence of a temperature gradient aligned with gravity. In fact, early attempts to gain insight into the characteristics of cross-field plasma dynamics considered purely paradigmatic models for two-dimensional thermal convection [13–17] (sometimes augmented by the inclusion of heuristic dissipation terms to account for the presence of particle sinks at the sheath of the SOL [18–21]). Although the analogy is not as straightforward as this, it can indeed be shown that simple SOL interchange models can be viewed as describing thermal convection augmented by additional effects [22].

Subsequently, motivated by the notion that SOL turbulence originates in the edge region (inside the separatrix), the simple SOL models have been extended to consider a configuration composed of the two regions (core and SOL — labelled B and A in Fig. 1), connected at the interface [23–29]. As described above, the two regions exhibit distinct dynamics parallel to the magnetic field. In the core, magnetic field lines are closed (periodic in the parallel direction), while in the SOL the field lines end at a material surface; the presence of the solid surface provides a sink for plasma particles and energy. Mathematically, the transition from closed to open field line regions in the models is

represented by pre-multiplying the parallel loss terms by a smooth step function. The separatrix position is fixed on the basis of the electrostatic approximation. The topological distinction between the core and SOL regions also has consequences for the perpendicular dynamics. In the toroidal plasma the expressions for perpendicular diffusion are given by neoclassical theory. In particular, the neoclassical expressions for particle diffusivity and viscosity are given by Ref. [25]

$$D^{neo} = (1 + 1.6q^2)D^{cl}, \qquad \mu^{neo} = (1 + 1.3q^2)\mu^{cl}, \tag{1}$$

where D^{cl} and μ^{cl} denote the classical values, and the quantity q is the so-called safety factor, which measures the pitch of the magnetic field. The theoretical framework used to derive expressions (1) relies on the existence of closed field lines to obtain the effective radial diffusivities. By contrast, we are interested in the values of these diffusivities in the region of plasma edge that spans both the closed and open field line regions. While there does not yet exist a theory of neoclassical transport on open field lines, it is conceivable that the values of transport coefficients in the SOL should lie between their classical and neoclassical values. The value of q depends on the machine (e.g. on MAST $q = 7$). Consequently, the neoclassical and classical values, and hence the diffusivities in the core and the SOL, can differ by one or two orders of magnitude.

Therefore, in the spirit of previous comparisons of single region plasma problems to single layer Rayleigh-Bénard convection, we may draw a similar analogy between two-region plasma models and two-layer convection — i.e. two-region plasma models can be viewed as a modified two-layer convection problem. The modifications arise in two ways: the first comes from the extra terms which account for plasma related effects; the second is due to interface conditions. In this paper we focus on the latter modification, and consider a simple two-layer convection model, as a precursor to the study of the more complicated core-SOL problem including all of the plasma-related effects. The superposed layers represent the core and the SOL, with the interface between the layers representing the separatrix. Conventionally, in two-layer convection, the layers are considered immiscible and an impermeability condition is enforced at the interface between the two fluids. When the interface is considered fixed flat this amounts to imposing the condition of vanishing vertical velocity. This forces convection to develop as two cells — one in each layer. A more relevant interface condition in the context of the core-SOL problem is the continuity of velocity, with plasma allowed to flow freely across the separatrix. With the immiscibility condition relaxed, two cells are no longer necessary, and convection can develop in the form of a single cell spanning the whole domain. Such a configuration is a special case of the problem studied by Le Bars and Davaille [30]. There, the two fluid layers were considered to be miscible in the sense that there was no surface tension at the interface. The only parameter that plays a role at the interface is the buoyancy number B — the ratio of chemical density anomaly to thermal density anomaly. In the limit of $B = 0$, the fluids in each layer are of equal density, and the interface conditions reduce to those in which we are interested. Whereas Le Bars and Davaille [30] only consider the effect of variation of viscosity contrast, and focus on the occurrence of the oscillatory instability for $B \neq 0$, here, motivated by the plasma problem, we are interested in the behavior of the system when both the viscosity and thermal diffusivity ratios between the layers vary by several orders of magnitude.

The remainder of the paper is structured as follows. Section II contains the mathematical formulation of the problem; in Section II A we introduce the governing equations, together with the conditions to be satisfied at the boundaries and at the interface; Section II B discusses characteristics of the marginal stability problem and Section II C reviews four previously studied limiting cases. Section III looks in detail at the onset of convection, particularly at the influence of the ratios of viscosity and thermal diffusivity; the case of equal layer depths is studied in Section III A, that of unequal depths in Section III B. A concluding discussion is contained in Section IV.

II. MATHEMATICAL FORMULATION

A. Governing equations

We consider two horizontal layers of fluid, one above the other, heated from below. Let d_1 and $d_2 = \delta d_1$ denote the depths of the lower and upper layers respectively. We assume that the fluid layers have kinematic viscosity ν_i, thermal diffusivity κ_i and coefficient of expansion γ_i, where index $i = 1$ refers to the lower layer and $i = 2$ to the upper layer. Let the lower layer occupy $-d_1 < z < 0$ and the upper $0 < z < d_2$. The planes $z = -d_1$ and $z = d_2$ are held at uniform temperatures T_b and T_u respectively, with $T_b > T_u$. A sketch of the configuration is shown in Fig. 2. A comparison of Fig. 1 and Fig. 2 leads to the identification of the lower layer with the core and the upper layer with the SOL. Prior to the onset of convection the fluid is at rest and the applied temperature difference imposes a conductive temperature profile in both layers:

$$T_1 = T_b - \beta_1(z + d_1), \qquad -d_1 \leq z < 0, \tag{2}$$

$$T_2 = T_u - \beta_2(z - d_2), \qquad 0 \leq z \leq d_2, \tag{3}$$

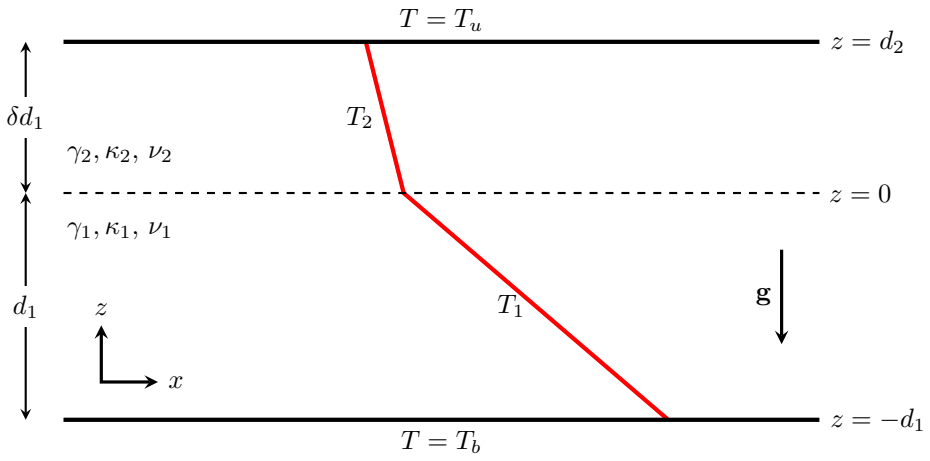

FIG. 2: Sketch of the problem configuration.

where β_i represent the adverse temperature gradient in each layer. Furthermore, continuity of temperature and heat flux require that

$$\beta_1 = \frac{\kappa_2(T_b - T_u)}{\kappa_2 d_1 + \kappa_1 d_2}, \qquad \beta_2 = \frac{\kappa_1(T_b - T_u)}{\kappa_2 d_1 + \kappa_1 d_2}. \tag{4}$$

Hence, the total temperature difference is split into a temperature drop across each layer, with the temperature drop in each layer related to the thermal diffusivities and depths of the two layers.

Under the Boussinesq approximation, the equation of motion for the velocity $\boldsymbol{u}_i$ and the heat equation for the temperature deviation θ_i from the steady state temperature distribution, for each fluid layer, are given by

$$\boldsymbol{\nabla} \cdot \boldsymbol{u}_i = 0, \tag{5}$$

$$\frac{\partial \boldsymbol{u}_i}{\partial t} + \boldsymbol{u}_i \cdot \boldsymbol{\nabla} \boldsymbol{u}_i = -\frac{1}{\rho_0} \boldsymbol{\nabla} p_i + \gamma_i g \theta_i \hat{\boldsymbol{e}}_z + \nu_i \nabla^2 \boldsymbol{u}_i, \tag{6}$$

$$\frac{\partial \theta_i}{\partial t} + \boldsymbol{u}_i \cdot \boldsymbol{\nabla} \theta_i = \beta_i w_i + \kappa_i \nabla^2 \theta_i. \tag{7}$$

We express the governing equations in dimensionless form: scaling time with d_1^2/κ_1, length with d_1, velocities $\boldsymbol{u}_i$ with κ_1/d_1, pressures p_i with $\rho_0(\kappa_1/d_1)^2$ and temperatures θ_i with $\beta_1 d_1$ yields the following dimensionless equations for each fluid layer:

$$\frac{\partial \boldsymbol{u}_1}{\partial t} + \boldsymbol{u}_1 \cdot \boldsymbol{\nabla} \boldsymbol{u}_1 = -\boldsymbol{\nabla} p_1 + Ra_1 Pr_1 \theta_1 \hat{\boldsymbol{e}}_z + Pr_1 \nabla^2 \boldsymbol{u}_1, \tag{8}$$

$$\frac{\partial \theta_1}{\partial t} + \boldsymbol{u}_1 \cdot \boldsymbol{\nabla} \theta_1 = w_1 + \nabla^2 \theta_1, \tag{9}$$

$$\frac{\partial \boldsymbol{u}_2}{\partial t} + \boldsymbol{u}_2 \cdot \boldsymbol{\nabla} \boldsymbol{u}_2 = -\boldsymbol{\nabla} p_2 + Ra_1 Pr_1 \frac{\gamma_2}{\gamma_1} \theta_2 \hat{\boldsymbol{e}}_z + \frac{\nu_2}{\nu_1} Pr_1 \nabla^2 \boldsymbol{u}_2, \tag{10}$$

$$\frac{\partial \theta_2}{\partial t} + \boldsymbol{u}_2 \cdot \boldsymbol{\nabla} \theta_2 = \frac{\beta_2}{\beta_1} w_2 + \frac{\kappa_2}{\kappa_1} \nabla^2 \theta_2, \tag{11}$$

where

$$Ra_1 = \frac{g \gamma_1 \beta_1 d_1^4}{\nu_1 \kappa_1}, \qquad Pr_1 = \frac{\nu_1}{\kappa_1}. \tag{12}$$

Since we are interested in the onset of infinitesimal disturbances, we linearize the governing equations (8)–(11), thereby neglecting the nonlinear terms $\boldsymbol{u}_i \cdot \boldsymbol{\nabla} \boldsymbol{u}_i$ and $\boldsymbol{u}_i \cdot \boldsymbol{\nabla} \theta_i$. Furthermore, we assume the flow to be two-dimensional and introduce streamfunctions ψ_i such that $\boldsymbol{u}_i = \boldsymbol{\nabla} \times (\psi_i \boldsymbol{e}_y)$ and the vorticity $\omega_i = -\nabla^2 \psi_i$. On taking the curl of

the momentum equations (8) and (10), the linearized forms of the equations of motion become

$$\frac{1}{Pr_1}\frac{\partial \omega_1}{\partial t} = -Ra_1\frac{\partial \theta_1}{\partial x} + \nabla^2\omega_1, \tag{13}$$

$$\frac{\partial \theta_1}{\partial t} = \frac{\partial \psi_1}{\partial x} + \nabla^2\theta_1, \tag{14}$$

$$\frac{1}{Pr_1}\frac{\partial \omega_2}{\partial t} = -Ra_1\gamma_r\frac{\partial \theta_2}{\partial x} + \nu_r\nabla^2\omega_2, \tag{15}$$

$$\frac{\partial \theta_2}{\partial t} = \beta_r\frac{\partial \psi_2}{\partial x} + \kappa_r\nabla^2\theta_2, \tag{16}$$

where $\kappa_r = \kappa_2/\kappa_1$, $\nu_r = \nu_2/\nu_1$, $\beta_r = \beta_2/\beta_1$, $\gamma_r = \gamma_2/\gamma_1$.

In dimensionless units, the lower layer occupies $-1 \le z < 0$, and the upper layer occupies $0 < z \le \delta$. The outer boundaries are assumed to be stress free and isothermal, thus

$$\psi_1 = \frac{\partial^2\psi_1}{\partial z^2} = \theta_1 = 0 \quad \text{at} \quad z = -1, \tag{17}$$

$$\psi_2 = \frac{\partial^2\psi_2}{\partial z^2} = \theta_2 = 0 \quad \text{at} \quad z = \delta. \tag{18}$$

At the boundary between the two layers, i.e. at $z = 0$, we assume the following continuity conditions. Continuity of velocity gives

$$\psi_1 = \psi_2, \quad \frac{\partial \psi_1}{\partial z} = \frac{\partial \psi_2}{\partial z}. \tag{19}$$

Continuity of tangential and normal stress yields

$$\nu_1\left(\frac{\partial^2\psi_1}{\partial z^2} - \frac{\partial^2\psi_1}{\partial x^2}\right) = \nu_2\left(\frac{\partial^2\psi_2}{\partial z^2} - \frac{\partial^2\psi_2}{\partial x^2}\right), \tag{20}$$

$$\nu_1\frac{\partial}{\partial z}\left(\frac{\partial^2\psi_1}{\partial z^2} + 3\frac{\partial^2\psi_1}{\partial x^2}\right) = \nu_2\frac{\partial}{\partial z}\left(\frac{\partial^2\psi_2}{\partial z^2} + 3\frac{\partial^2\psi_2}{\partial x^2}\right). \tag{21}$$

It is important to note that an unavoidable consequence of the conditions of continuity of tangential and normal stress, (20) and (21), is a discontinuity in vorticity across the interface for $\nu_r \neq 1$. Finally, continuity of temperature and heat flux lead to

$$\theta_1 = \theta_2, \quad \kappa_1\frac{\partial \theta_1}{\partial z} = \kappa_2\frac{\partial \theta_2}{\partial z}. \tag{22}$$

B. Marginal stability analysis

We seek normal mode solutions of the form

$$\psi_i = \hat{\psi}_i(z)\exp(ikx + \sigma t) + c.c., \tag{23}$$

$$\theta_i = \hat{\theta}_i(z)\exp(ikx + \sigma t) + c.c., \tag{24}$$

where k is the horizontal wavenumber and σ is the growth rate. Substituting these expressions into equations (13)–(16) yields

$$\frac{\sigma}{Pr_1}(\mathcal{D}^2 - k^2)\psi_1 = ik\,Ra_1\theta_1 + (\mathcal{D}^2 - k^2)^2\psi_1, \tag{25}$$

$$\sigma\theta_1 = ik\,\psi_1 + (\mathcal{D}^2 - k^2)\theta_1, \tag{26}$$

$$\frac{\sigma}{Pr_1}(\mathcal{D}^2 - k^2)\psi_2 = ik\,Ra_1\gamma_r\theta_2 + \nu_r(\mathcal{D}^2 - k^2)^2\psi_2, \tag{27}$$

$$\sigma\theta_2 = ik\beta_r\psi_2 + \kappa_r(\mathcal{D}^2 - k^2)\theta_2, \tag{28}$$

where $\mathcal{D}$ denotes differentiation with respect to z. The boundary and interface conditions (17)–(22) may be written as

$$\psi_1 = \mathcal{D}^2\psi_1 = \theta_1 = 0 \quad \text{at} \quad z = -1, \tag{29}$$

$$\psi_2 = \mathcal{D}^2\psi_2 = \theta_2 = 0 \quad \text{at} \quad z = \delta, \tag{30}$$

$$\psi_1 = \psi_2, \quad \mathcal{D}\psi_1 = \mathcal{D}\psi_2,$$

$$\left(\mathcal{D}^2\psi_1 + k^2\psi_1\right) = \nu_r\left(\mathcal{D}^2\psi_2 + k^2\psi_2\right),$$

$$\left(\mathcal{D}^3\psi_1 - 3k^2\mathcal{D}\psi_1\right) = \nu_r\left(\mathcal{D}^3\psi_2 - 3k^2\mathcal{D}\psi_2\right),$$

$$\theta_1 = \theta_2, \quad \mathcal{D}\theta_1 = \kappa_r\mathcal{D}\theta_2 \quad \text{at} \quad z = 0. \tag{31}$$

As described in the Introduction (Section I), the problem formulated here is a special case of that studied in Ref. [30]. There, the fluid layers were considered to have different densities, thus introducing the additional parameter B, a ratio of two density differences, one of chemical and one of thermal origin. The two problems are equivalent when $B = 0$. In general, depending on the value of B, the solutions at the onset of instability are either steady or oscillatory. In particular, oscillatory instability sets in for $0 < B < B_c$, where B_c is some critical value; for $B > B_c$ the most unstable mode has purely real growth rate. Similarly, in the absence of density stratification, i.e. in the limit $B = 0$, the frequency at the onset of instability vanishes and the oscillatory mode transforms itself into a steady mode. Therefore, we restrict attention to the onset of stationary convection, in which case $\sigma = 0$. Consequently, the Prandtl number Pr_1 does not enter the analysis. It follows from (4) that $\beta_r = \kappa_r^{-1}$; furthermore, we fix $\gamma_r = 1$. Our task has thus been reduced to the problem of determining the critical conditions as a function of the parameters δ, ν_r and κ_r. Moreover, we observe that the equations are identical on interchanging (Ra_1, δ, ν_r, κ_r) and (Ra_2, δ^{-1}, ν_r^{-1}, κ_r^{-1}), where Ra_2 is the Rayleigh number of the upper layer, defined by

$$Ra_2 = \frac{g\gamma_2\beta_2(\delta d_1)^4}{\nu_2\kappa_2} = \frac{Ra_1\delta^4}{\nu_r\kappa_r^2}. \tag{32}$$

Therefore, we need only consider the case with $\delta \leq 1$; the case with $\delta > 1$ can be reconstructed from symmetry considerations.

The ratio Ra_2/Ra_1 provides a measure of the ratio of the contributions from the two layers to the buoyancy-driven instability. When this ratio is significantly different from unity, the onset of instability occurs primarily in one layer, while the other plays a passive role [6]. Clearly, this will be the case when either ν_r or κ_r (or both) are either very small or very large. Note, however, that it is not instructive to consider either of the Rayleigh numbers individually. For example, consider the case of layers of equal depth and viscosity ($\delta = \nu_r = 1$) and large thermal diffusivity contrast. Recall from (4) that the basic state temperature gradients in each layer are

$$\beta_1 = \frac{\Delta T}{d_1\left(1 + \kappa_r^{-1}\delta\right)}, \qquad \beta_2 = \frac{\Delta T}{\delta d_1\left(1 + \kappa_r\delta^{-1}\right)}, \tag{33}$$

where $\Delta T = (T_b - T_u)$. It follows that as $\kappa_r \to 0$, $\beta_1 \to 0$ and $\beta_2 \to \Delta T/\delta d_1$. Thus the entire temperature drop occurs over the upper layer, while in the bottom layer there is no buoyancy and consequently $Ra_1 \to 0$. This should not be taken to mean that layer 1 becomes unstable even in the absence of an adverse thermal gradient, but rather that layer 1 does not contribute to the onset of instability. Conversely, when $\kappa_r \to \infty$, $\beta_1 \to \Delta T/d_1$ and $\beta_2 \to 0$; thus layer 1 is entirely responsible for the onset of instability, while layer 2 plays a passive role.

C. Limiting cases

We note that when the fluid properties of each layer are equal (i.e. $\nu_r = \kappa_r = 1$) then the problem reduces to that of classical (single layer) Rayleigh-Bénard convection, with the onset of instability occurring at

$$Ra_1^c = \frac{27}{4}\left(\frac{\pi}{1+\delta}\right)^4, \qquad k^c = \frac{1}{\sqrt{2}}\left(\frac{\pi}{1+\delta}\right). \tag{34}$$

On the other side of the spectrum, the problem we wish to study has four interesting limits:

1. when one of the layers is infinitely more viscous than the other, i.e. $\nu_r \to \infty$ (or $\nu_r \to 0$);

2. when one of the layers is infinitely more thermally diffusive than the other, i.e. $\kappa_r \to \infty$ (or $\kappa_r \to 0$);

3. when one of the layers is both infinitely more viscous and thermally diffusive than the other, i.e. $\kappa_r \to \infty$, $\nu_r \to \infty$ (or $\kappa_r \to 0$, $\nu_r \to 0$);

4. when one of the layers is infinitely more viscous and the other is infinitely more thermally diffusive, i.e. $\kappa_r \to 0$, $\nu_r \to \infty$ (or $\kappa_r \to \infty$, $\nu_r \to 0$).

Three of these cases (1, 3 and 4) can be understood by considering the limits in the problem of Nield [31], who studied the onset of stationary convection in a layer of fluid, of depth d and thermal conductivity K, bounded from below by a rigid plate of infinite thermal conductivity and from above by a solid layer of finite conductivity K' and finite thickness d'. The fluid layer is governed by the steady version of equations (13) and (14), while the solid layer obeys $\nabla^2\theta = 0$. The no-slip condition is applied on the boundaries of the fluid layer: i.e. at the bottom plate and at the fluid-solid boundary. The thermal boundary conditions consist of fixed temperature at the bottom of the fluid and at the top of the solid, and continuity of temperature and heat flux at the fluid-solid interface.

Nield [31] calculated the critical Rayleigh number as a function of the depth ratio d'/d and thermal conductivity ratio K'/K (these are analogous to parameters δ and κ_r in our problem). The two limiting cases of interest are: $K'/K \to 0$, and $K'/K \to \infty$. When $K'/K \to \infty$, the critical Rayleigh number and the critical wavenumber tend to

$$Ra = 1707.8, \qquad k = 3.117. \tag{35}$$

These correspond to the onset of convection in a layer bounded by rigid isothermal plates. This makes sense: when K' is infinite, the boundary condition at the top of the solid is instantaneously transmitted throughout the solid, to the top of the fluid.

The second limit is slightly more subtle. When $K'/K \to 0$, the critical Rayleigh number and the critical wavenumber tend to

$$Ra = 1295.8, \qquad k = 2.553. \tag{36}$$

These values correspond to those of the onset of convection in a layer where one boundary is rigid and isothermal and the other is rigid with constant heat flux. As $K'/K \to 0$, the condition of contuinuty of heat flux at the fluid-solid boundary becomes the condition of no heat flux and the solid layer becomes a perfect insulator.

III. ONSET OF CONVECTION

A. The case of equal layer depths ($\delta = 1$)

We now return to the problem governed by equations (25)–(31). We begin with the case of two layers of equal depth, i.e. $\delta = 1$, and equal thermal diffusivity, $\kappa_r = 1$, and consider the effect of varying the viscosity ratio ν_r. Figure 3 shows the variation of the critical Rayleigh numbers, Ra_1^c and Ra_2^c, and the critical wavenumber k^c with respect to ν_r. As discussed in Section II B, the symmetry of the system with $\delta = 1$ results in a reflectional symmetry (when ν_r is plotted logarithmically) between the Ra_1^c and Ra_2^c curves about the line $\nu_r = 1$. Similarly, k^c is symmetric about $\nu_r = 1$.

Perhaps the most striking feature of Fig. 3(b) is the non-monotonic behavior of the critical wavenumber k. When $\nu_r = 1$ (i.e. single layer convection), the convection cells fill the entire depth of the domain, with horizontal length scale given by (34). On first introducing a viscosity contrast between the two layers — and here we consider $\nu_r > 1$, without loss of generality — there is an initial decrease in the critical wavenumber, indicating a shift in the preferred horizontal length scale toward larger cells. This is accompanied by a decrease in Ra_2 and an increase in Ra_1, thereby indicating the growing importance of the lower layer in terms of contributing to the instability. On increasing the viscosity ratio further, there is a marked transition, with a sharp increase in the critical wavenumber. At this point the convective cells are expelled from the viscous layer, and the motion is localized in the layer with lower viscosity, as seen in Fig. 4. It is interesting to note that similar localized solutions have been observed in the problem of single layer convection in which the viscosity is a strongly but smoothly varying function of temperature; there the convection becomes confined to a sublayer as the ratio of maximum to minimum viscosity increases. ADD REFERENCES.

As the viscosity contrast becomes infinite, the interface behaves like a rigid boundary, and the viscous layer like a solid slab. The critical Rayleigh number of the less viscous layer and the critical wavenumber tend towards asymptotic values, which correspond to those of convection in a layer of fluid in which one boundary is a solid layer of finite thermal conductivity and thickness; on this boundary the velocity obeys the no-slip condition. Hence, in this limit, the problem is reduced to that studied in Ref. [31], although there the other boundary was assumed to be rigid (no-slip), whereas here it is stress free. Naturally, the Rayleigh number of the more viscous layer decreases indefinitely according

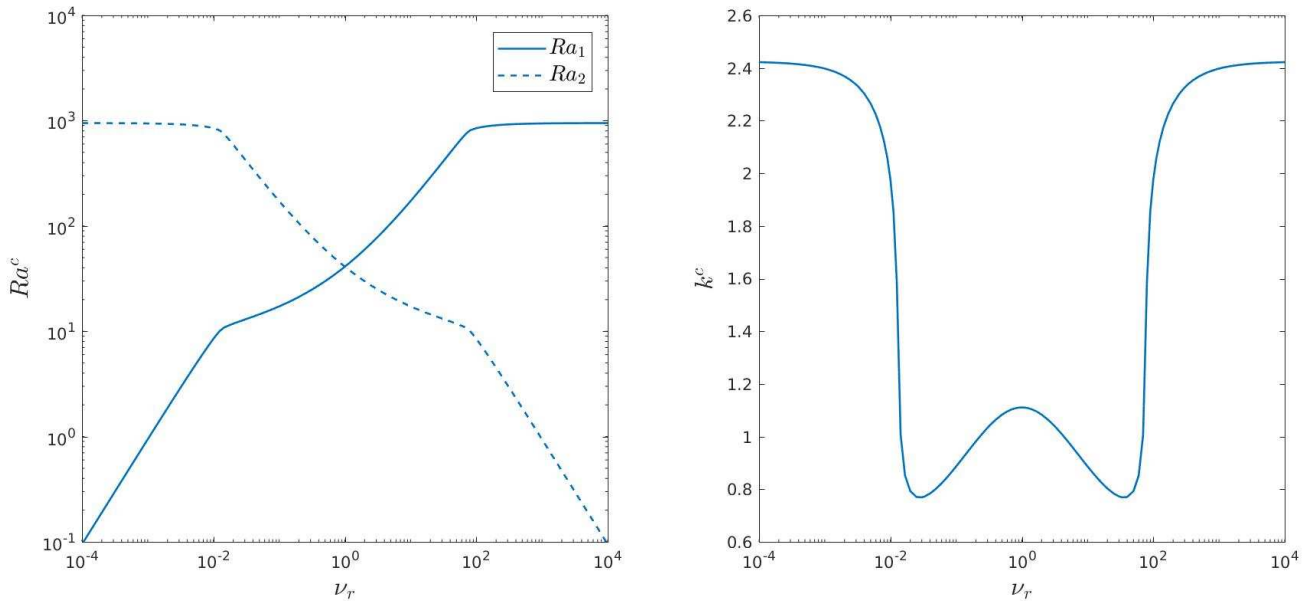

(a) (b)

FIG. 3: Variation of the critical Rayleigh number and the accompanying critical wavenumber as a function of ν_r, for the case of layers of equal depth and equal thermal diffusivity ($\delta = \kappa_r = 1$).

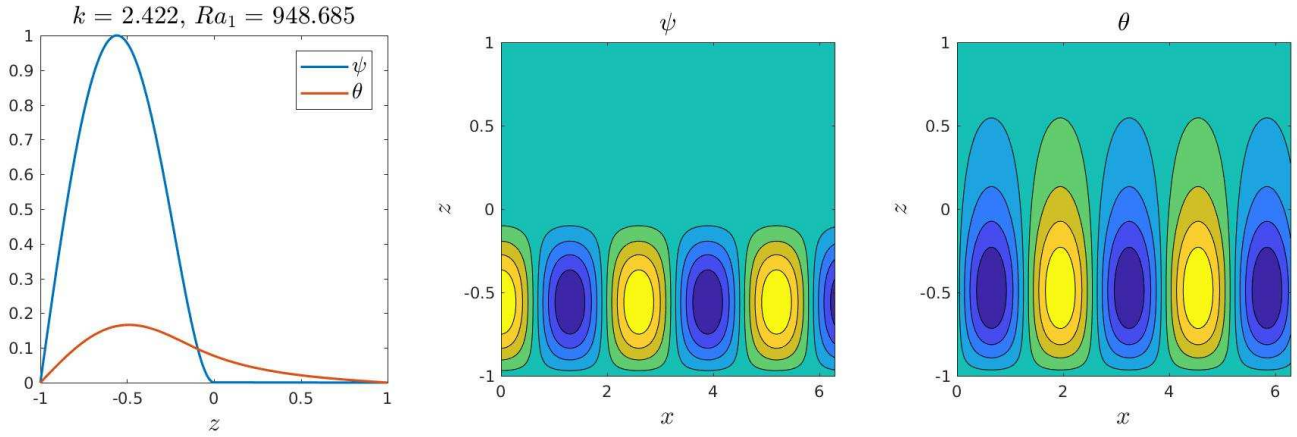

(a) (b) (c)

FIG. 4: Critical mode for $\nu_r = 10^4$, $\kappa_r = 1$, $\delta = 1$. (a) Eigenfunction profiles; (b) contour plot of the streamfunction; (c) contour plot of the temperature perturbation.

to relation (32). As noted earlier, this does not mean that the viscous layer becomes increasingly more unstable, but rather that the motion in this layer ceases, with the dynamics governed solely by the diffusion of the temperature perturbation.

The variation of Ra^c and k^c with respect to κ_r for the case of layers of equal viscosity, i.e. $\nu_r = 1$, is shown in Fig. 5. Similarly to the limit of infinite viscosity contrast described above, as the ratio of thermal diffusivities becomes infinite, the critical Rayleigh number and the critical wavenumber of the less thermally diffusive layer tend towards asymptotic values. Similarly, the Rayleigh number of the layer with higher thermal diffusivity decreases indefinitely according to expression (32). In this case, as the ratio of thermal diffusivities becomes infinite, the adverse temperature gradient in the thermally diffusive layer vanishes (cf. (33)), which necessitates vanishing Rayleigh number. The isothermal

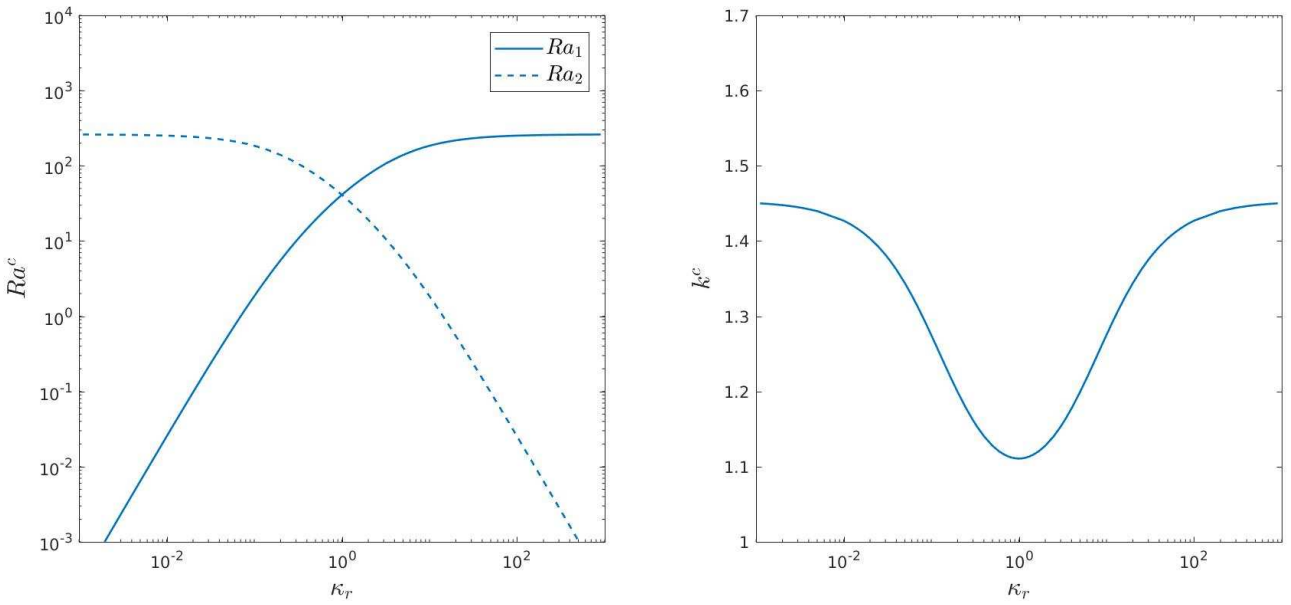

(a) (b)

FIG. 5: Variation of the critical Rayleigh number and critical wavenumber as a function of κ_r, for the case of layers of equal depth and equal viscosity ($\delta = \nu_r = 1$).

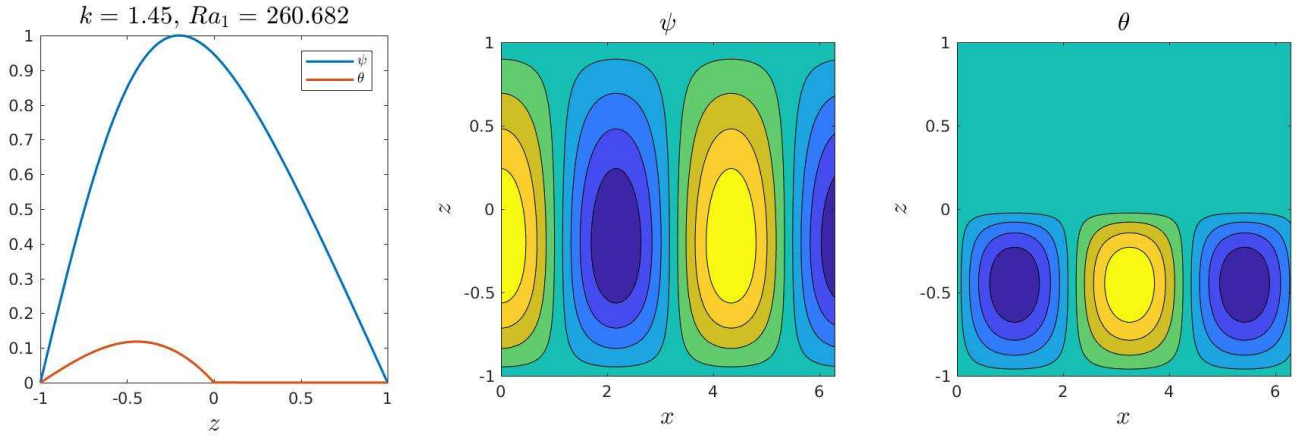

(a) (b) (c)

FIG. 6: Critical mode for $\kappa_r = 10^3$, $\nu_r = 1$, $\delta = 1$. (a) Eigenfunction profiles; (b) contour plot of the streamfunction; (c) contour plot of the temperature perturbation.

boundary condition is transmitted instantaneously throughout the thermally diffusive layer, and consequently the temperature perturbation is localized in the layer with lower thermal diffusivity, as can be seen in Fig. 6. Note, however, that the fluid motion persists in the thermally diffusive layer. Furthermore, the horizontal wavelength given by the asymptotic value of k^c as κ_r approaches either zero or infinity is representative of the vertical extent of the fluid motion. The motion in the thermally diffusive layer is of Stokes flow type (governed by $\nabla^2\nabla^2\psi = 0$) and is driven entirely by the mechanical forcing at the interface.

Figure 7 shows the variation of Ra^c and k^c with respect to ν_r at different values of κ_r. Clearly, the non-monotonic behavior of the wavenumber as a function of ν_r persists for values of κ_r other than unity. In fact it becomes more intricate, being dependent on whether the more (less) viscous layer is also more (less) thermally diffusive — i.e. if ν_r

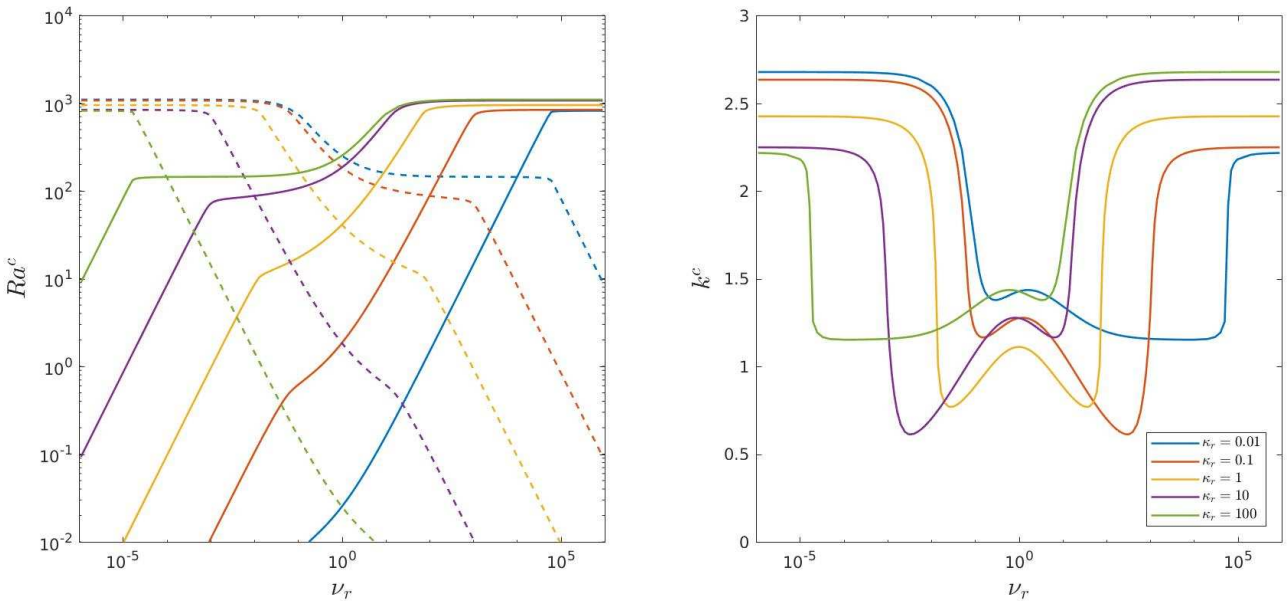

(a) (b)

FIG. 7: Variation of the critical Rayleigh numbers (solid lines denote Ra_1^c, dashed lines denote Ra_2^c) and critical wavenumber as a function of ν_r for different values of κ_r, with $\delta = 1$.

and κ_r are both less than 1, or both greater than 1.

If $\kappa_r > 1$, then initially as ν_r is increased from 1, k^c is reduced until it reaches a minimum, after which a further increase leads to a sharp increase in k^c towards an asymptotic limit. The position of the minimum of k^c, and the subsequent sharp transition, occurs at lower values of ν_r for higher values of κ_r. Furthermore, the initial dip in k^c is smaller for higher values of κ_r. As $\nu_r \to \infty$, the limiting values of the critical Rayleigh number of the less viscous layer (in this case the bottom layer) and the critical wavenumber increase with κ_r. The behavior of the limits of k^c and Ra^c as $\nu_r \to \infty$ is consistent with the results of Ref. [31], where it was also observed that both k^c and Ra^c increase as the ratio of solid to fluid conductivity is increased.

By analogy with the limits of Ref. [31], keeping ν_r infinite and allowing $\kappa_r \to \infty$, the viscous slab becomes infinitely conducting and so, in addition to acting like a no-slip boundary, the interface now also becomes isothermal. The asymptotic values of the critical Rayleigh number and the critical wavenumber correspond to those of single layer convection with fixed temperature boundaries of which one is rigid and the other is stress free [32]:

$$R_*^c = 1101, \qquad k_*^c = 2.67. \tag{37}$$

In this limit, both the convection cell and the temperature perturbation occupy the layer with lower viscosity and lower thermal diffusivity, as seen in Fig. 8. This picture changes slightly when the more viscous layer is less thermally diffusive. For $\kappa_r < 1$, as ν_r is increased from 1, there is an initial small increase in k^c, followed by a decrease in k^c to a minimum, and a subsequent sharp increase towards the asymptotic limit of $\nu_r \to \infty$. Additionally, the minimum of k^c moves to higher values of ν_r for smaller κ_r.

We have seen above (Fig. 4) that when the viscosity contrast is sufficiently large then the convective cells become localized in the layer with lower viscosity, while the other layer behaves like a solid slab. Similarly, for large enough thermal diffusivity contrast (Fig. 6), the temperature perturbation becomes confined to the less thermally diffusive layer. Interestingly, there is a regime in parameter space, with ν_r large and κ_r small, in which these pictures can be combined such that the critical mode is one in which fluid motion and temperature perturbation are segregated — i.e. confined to different layers. An example of such a mode is plotted in Fig. 9, where $\nu_r = 5 \times 10^4$ and $\kappa_r = 0.01$. However, this mode does not persist in the limit $\nu_r \to \infty$ and $\kappa_r \to 0$. On increasing ν_r, eventually there is a sharp increase in k^c (cf. Fig. 7) and the critical mode transitions towards the $\nu \to \infty$ limit: i.e. that corresponding to the critical mode of convection in a layer of fluid in which one boundary is a solid slab of finite thermal conductivity and thickness. In the limit $\nu_r \to \infty$ and $\kappa_r \to 0$, the viscous slab behaves like a perfect insulator and the thermal

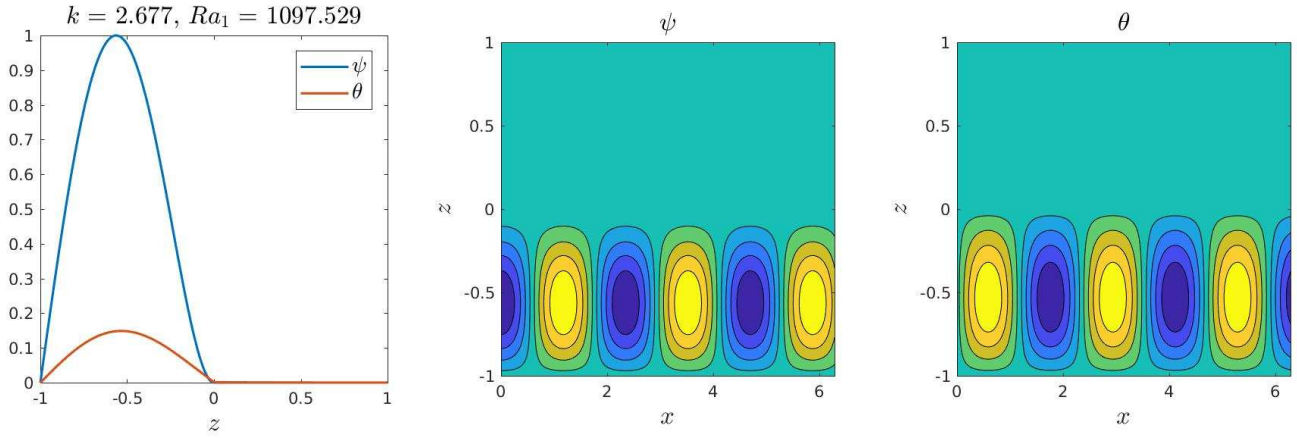

(a) (b) (c)

FIG. 8: Critical mode for $\kappa_r = 100$, $\nu_r = 9 \times 10^5$, $\delta = 1$. (a) Eigenfunction profiles; (b) contour plot of the streamfunction; (c) contour plot of the temperature perturbation.

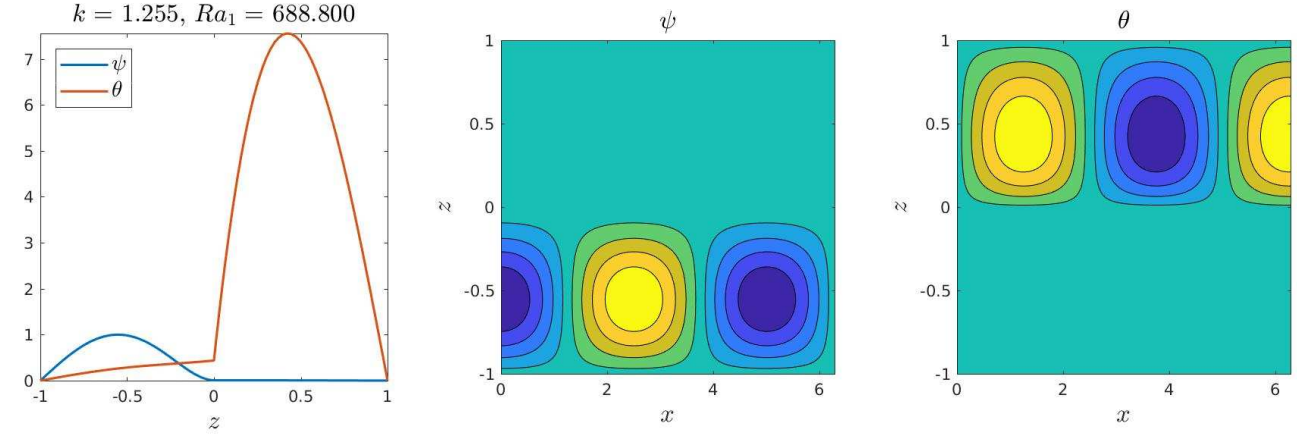

(a) (b) (c)

FIG. 9: Critical mode for $\kappa_r = 0.01$, $\nu_r = 5 \times 10^4$, $\delta = 1$. (a) Eigenfunction profiles; (b) contour plot of the streamfunction; (c) contour plot of the temperature perturbation.

condition on the interface is that of no heat flux. The limiting values of the critical Rayleigh number and the critical wavenumber correspond to those of single layer convection in which one of the boundaries is rigid and insulating, and the other is stress free and isothermal:

$$R_*^c = 816.75, \qquad k_*^c = 2.215. \tag{38}$$

B. The case of different layer depths ($\delta \neq 1$)

We now consider the case where the two layers are of different depth. As noted in Section II, the symmetry of the problem allows us to restrict attention to the case with $\delta < 1$, which means that the top layer will always be thinner than the bottom layer. We note that the interpretation of the limiting behavior of the critical Rayleigh number and the critical wavenumber with respect to ν_r and κ_r described above also holds in the case of layers of unequal depth. Additionally, in the limit $\delta \to 0$, Ra^c and k^c tend to the asymptotic values given by (37).

Figure 10 shows the variation of the critical Rayleigh numbers, Ra_1^c and Ra_2^c, with respect to the viscosity contrast ν_r for different values of layer depth ratio δ, with $\kappa_r = 1$. First, we consider the case with $\nu_r > 1$, i.e. the thin

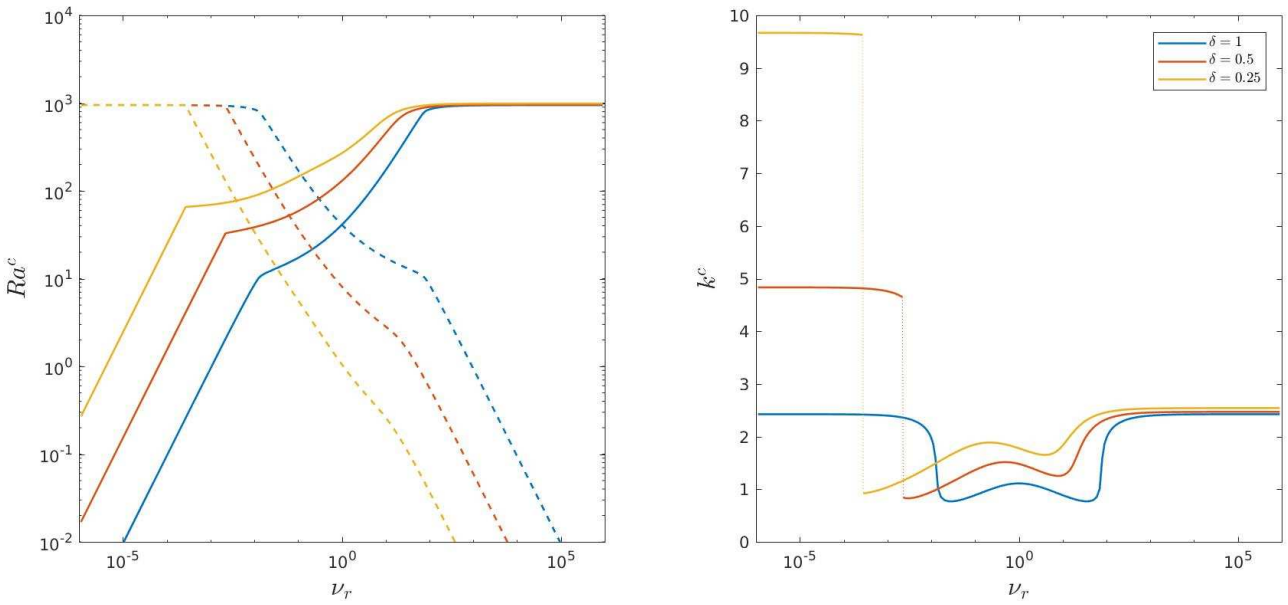

(a) (b)

FIG. 10: Variation of the critical Rayleigh number (solid lines denote Ra_1^c, dashed lines denote Ra_2^c) and critical wavenumber as a function of ν_r for different values of δ with $\kappa_r = 1$.

upper layer is more viscous. The behavior of the critical Rayleigh number and the critical wavenumber in the cases of unequal layer depths ($\delta = 0.25$ and $\delta = 0.5$) is qualitatively similar to that in the case of equal layer depths ($\delta = 1$). When $\nu_r = 1$, the convective cell fills the entire domain, and its horizontal scale, with critical wavenumber k^c given by expression (34), is comparable with the depth of the box. Initially, as ν_r is increased, k^c is reduced until it reaches a minimum. A further increase in ν_r leads to an increase in k^c towards an asymptotic limit, where the top layer behaves like a solid slab. This increase in k^c becomes less sharp, and occurs at lower values of ν_r, for smaller δ. The asymptotic values of Ra_1^c and k^c in the limit $\nu_r \to \infty$ increase as δ is decreased. This is consistent with the results of Ref. [31], in which it was also observed that both Ra^c and k^c increase with a decrease in the ratio of the depth of the solid layer to that of the fluid layer.

When $\nu_r < 1$, the thick bottom layer is more viscous, behaving like a solid slab when the viscosity contrast is sufficiently large. The value of ν_r at which the transition to this limiting behavior takes place decreases with decreasing δ. Furthermore, in the case of layers of unequal depth (i.e. $\delta \neq 1$) the transition becomes a discontinuous jump. At the point of discontinuity the marginal stability curve has two distinct minima, as seen in Fig. 11. Therefore, at the transition point, there are two distinct unstable modes. At the minimum corresponding to the lower wavenumber, the convective cell fills the entire domain, as can be seen in Fig. 12, with a horizontal scale comparable with that of the depth of the box. By contrast, at the minimum corresponding to the larger wavenumber, the motion is localized in the layer with lower viscosity, as seen in Fig. 13. The horizontal scale of convection cells in this case is comparable with the depth of the thin upper layer.

Figures 14, 15 show the variation of the critical Rayleigh numbers and the critical wavenumber with respect to ν_r, with $\kappa_r = 0.1$ and $\kappa_r = 10$ respectively. As in the case of equal layer depths ($\delta = 1$), the position of the minimum of the sharp transition in k^c shifts to lower values of ν_r as κ_r is increased.

IV. DISCUSSION

In this paper we have studied the linear stability of a two-layer Boussinesq convection problem in order to gain insight into the onset of interchange instability in two-region models of the plasma edge in fusion confinement devices. A key difference between the model that we have studied here and two-layer problems that have been considered previously is in the choice of interface conditions. Whereas conventionally the two layers are considered immiscible,

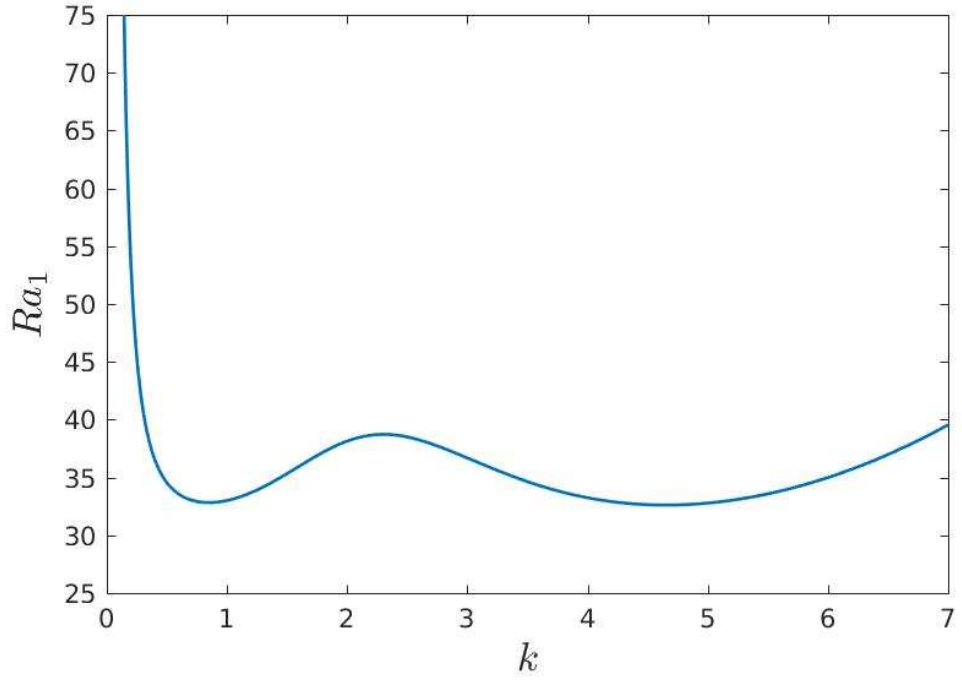

FIG. 11: Marginal stability curves for the case $\delta = 0.5$, $\nu_r = 2.2 \times 10^{-3}$, $\kappa_r = 1$.

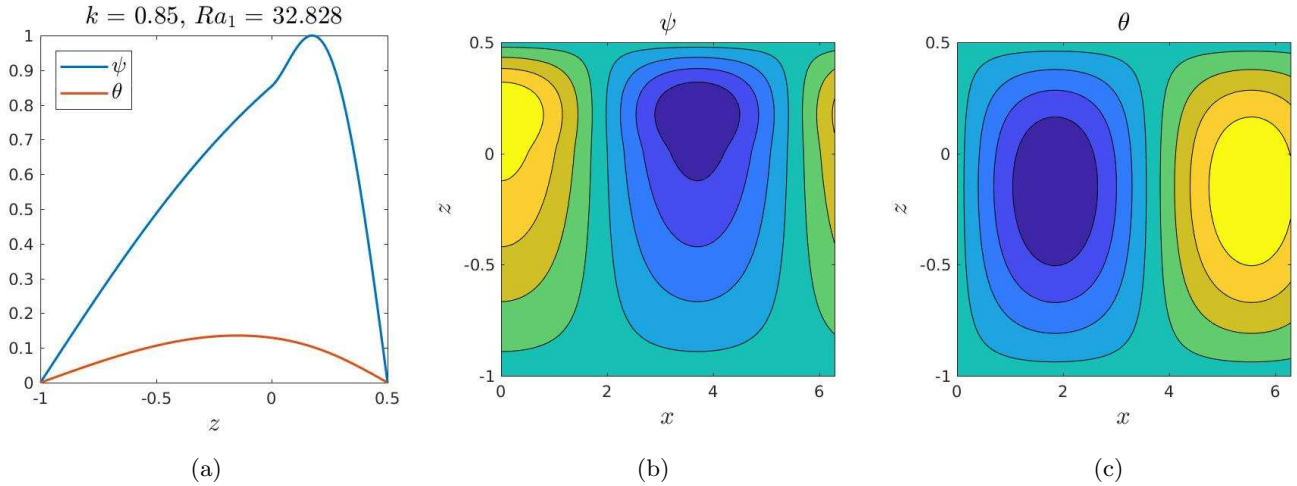

(a) (b) (c)

FIG. 12: Solution associated with the minimum at $k = 0.85$ of the marginal stability curve in Fig. 11. (a) Eigenfunction profiles; (b) contour plot of the streamfunction; (c) contour plot of the temperature perturbation.

separated by an impermeable interface, in the context of the core-SOL problem the relevant condition at the boundary between the two layers is the continuity of velocity, with plasma allowed to flow freely across the separatrix. The edge plasma problem can therefore be thought of as convection with a jump in viscosity and thermal diffusivity.

We have investigated the onset of convection as a function of viscosity contrast, thermal diffusivity contrast and layer depth ratio. Even in the fairly simple system considered here, depending on the values of these parameters, we have found a variety of distinct unstable modes. These can be broadly categorized according to three regimes: whole layer, localized, and segregated. The approximate boundaries between these regimes in (ν_r, κ_r) parameter space for the two cases of $\delta = 1$ and $\delta = 0.5$ are shown in Fig. 16; it can be seen that the regime diagrams for equal and unequal layer depths are qualitatively similar.

The whole layer regime occurs when neither the viscosity contrast, nor the thermal diffusivity contrast, are too

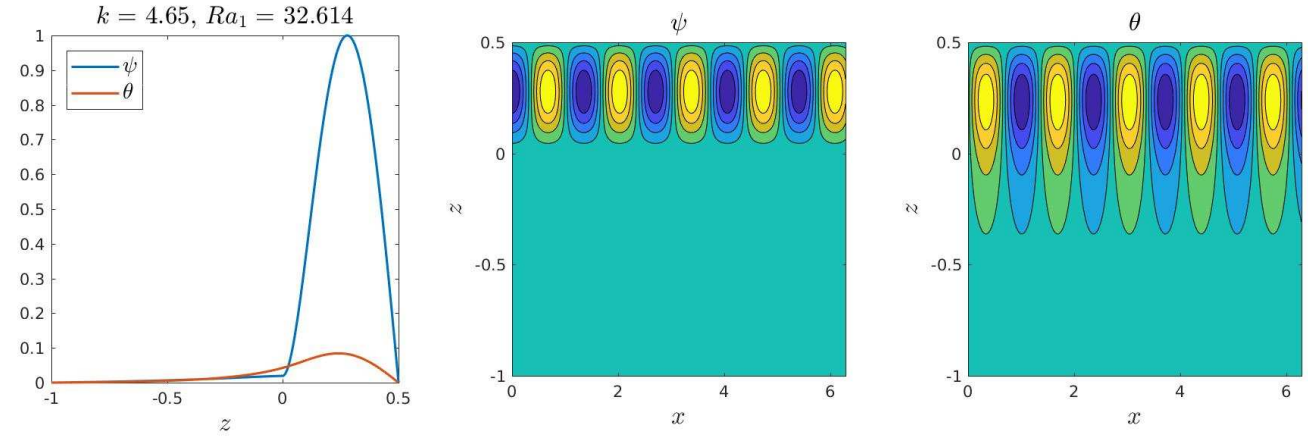

(a) (b) (c)

FIG. 13: Solution associated with the minimum at $k = 4.65$ of the marginal stability curve in Fig. 11. (a) Eigenfunction profiles; (b) contour plot of the streamfunction; (c) contour plot of the temperature perturbation.

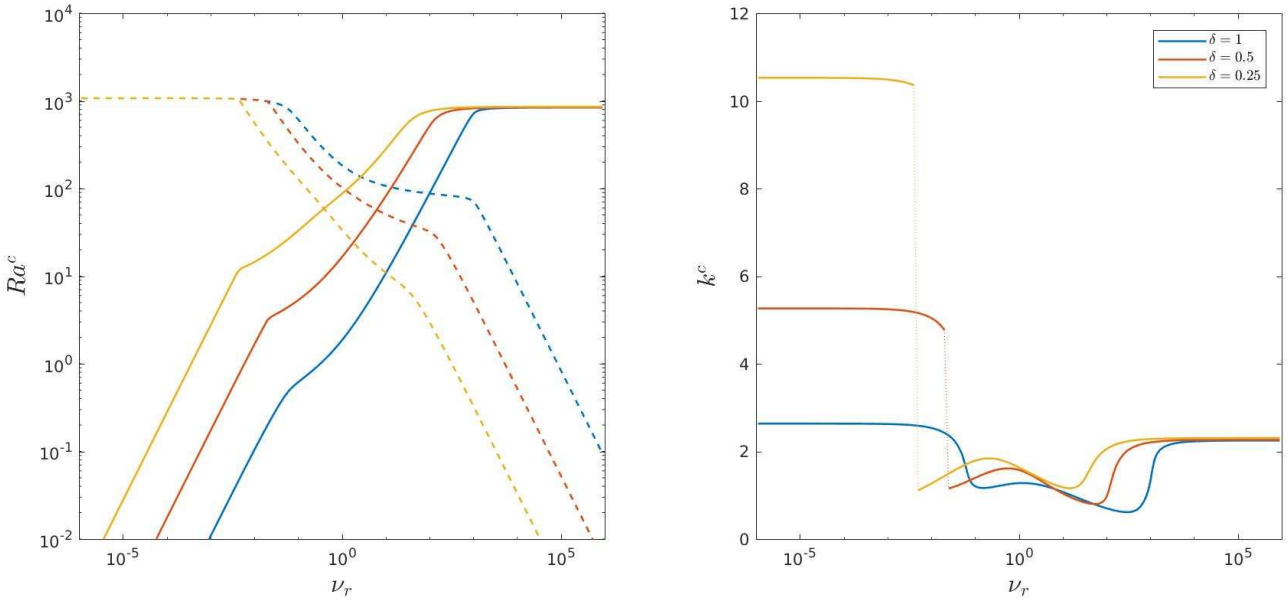

(a) (b)

FIG. 14: Variation of the critical Rayleigh number (solid lines denote Ra_1^c, dashed lines denote Ra_2^c) and critical wavenumber as a function of ν_r for different values of δ, with $\kappa_r = 0.1$.

large (region I in Fig. 16). In this regime, both the convection cells and the temperature perturbation extend over the two layers.

The localized modes are characterized by either the velocity cells, or the temperature perturbations, or both, being confined to one of the layers. In this regime, one of the layers is entirely responsible for the onset of instability, while the other plays a passive role. The localized solutions are associated with limits of infinite viscosity contrast and infinite thermal diffusivity contrast, and can be further sub-categorized accordingly. In the regime associated with the limit of infinite viscosity contrast (region IIb), the viscous layer behaves like a solid slab; the convection cells become localized to the layer with lower viscosity, and the temperature perturbation penetrates the viscous layer only through diffusion. In the regime associated with the limit of infinite thermal diffusivity contrast (region IIa), the

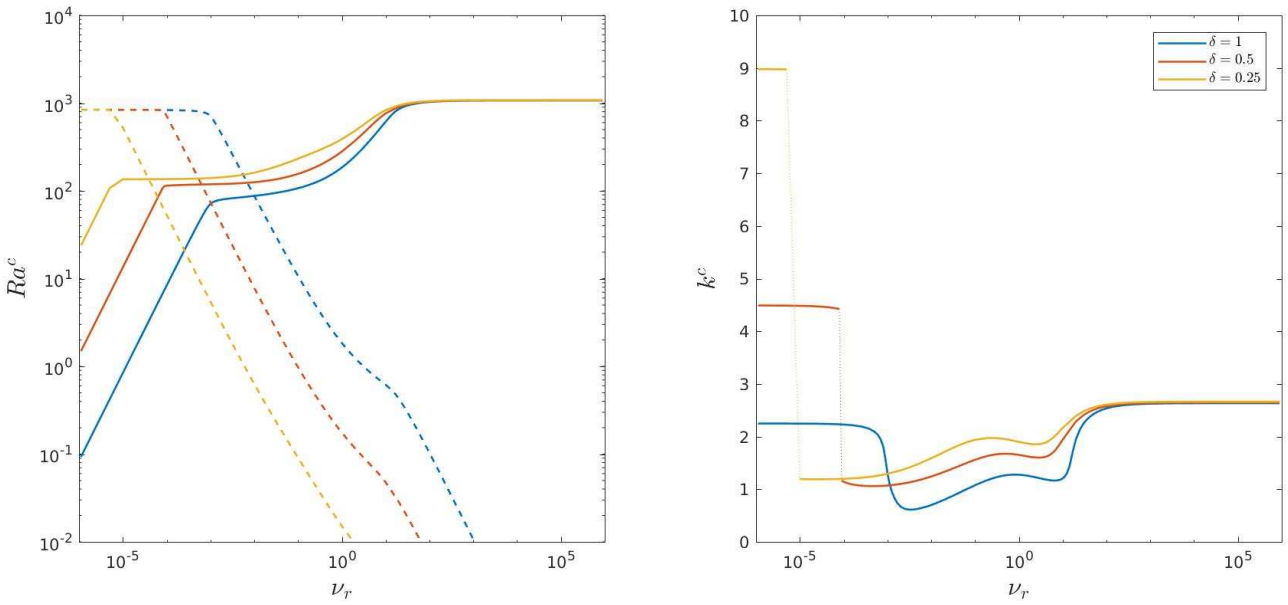

(a) (b)

FIG. 15: Variation of the critical Rayleigh number (solid lines denote Ra_1^c, dashed lines denote Ra_2^c) and critical wavenumber as a function of ν_r for different values of δ, with $\kappa_r = 10$.

temperature perturbation is confined to the layer with lower thermal diffusivity. In the layer with higher thermal diffusivity, there is no buoyancy, owing to the absence of thermal gradient, and the fluid motion is forced entirely through the mechanical coupling at the interface. Naturally, on intersection of the regimes associated with $\kappa_r \to \infty$ and $\nu_r \to \infty$ (or $\kappa_r \to 0$ and $\nu_r \to 0$) — i.e. when one of the layers is both significantly more viscous and thermally diffusive — both the velocity and the temperature perturbation of the most unstable mode are localized to the less diffusive layer (region IIab). The transition between the whole-layer and the localized regimes is governed by the ratio of the Rayleigh numbers. Although the precise critical value of that ratio depends nonlinearly on ν_r, κ_r and δ, and is impossible to extract analytically, in general it seems that one of the Rayleigh numbers must be sufficiently greater than the other.

The segregated regime occurs when one of the layers is significantly more viscous, while the other is significantly more thermally diffusive (region III). The critical mode is one where the fluid motion and the temperature perturbation are segregated, being confined, respectively, to layers with lower viscosity and lower thermal diffusivity.

Although two-layer convection is an idealization of the core-SOL interaction, it is nonetheless of interest to try to place our results in the context of the full plasma problem. As discussed in the Introduction, the particle diffusivity and viscosity may differ considerably between the core and the SOL; if this is the case this would lead to a regime with $\nu_r \ll 1$ and $\kappa_r \ll 1$, with both the velocity and the temperature perturbation confined to the SOL. It is tempting to speculate that the filaments observed to propagate radially at the edge of tokamaks are nonlinear manifestations of these localized modes. It should however be borne in mind that the purely convective model does not include all of the physical effects present in the full plasma problem. Specifically there are two types of modification required. One is the addition of extra features accounting for plasma-related effects that act over both layers — these include a non-uniform basic state gradient and additional advective terms. The other is the physical representation of particle and energy losses in the regions of open field lines; this requires the inclusion of additional linear damping terms in the equations governing the SOL. This latter modification breaks the symmetry of the problem, and possibly inhibits the existence of modes localised to the SOL. In order to pursue these questions, we are currently investigating the full two-region plasma problem.

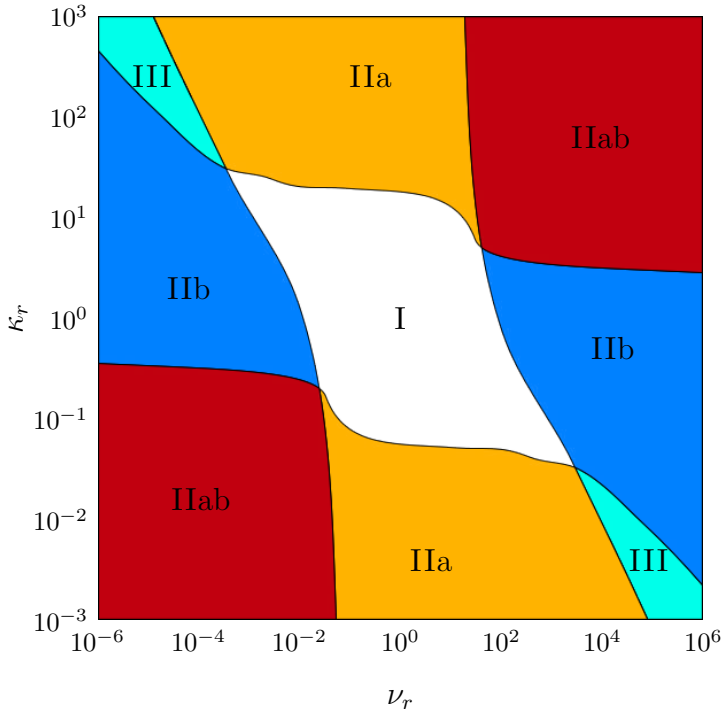

(a) $\delta = 1$

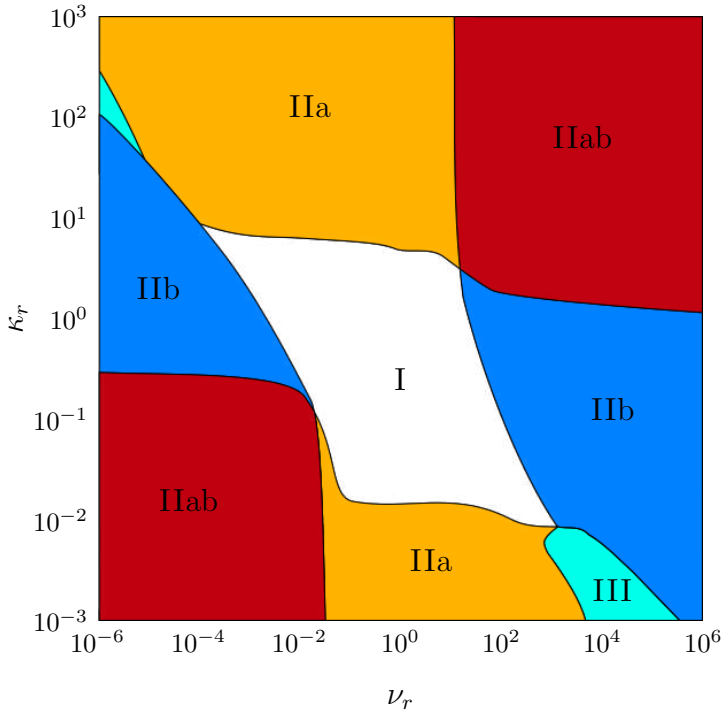

(b) $\delta = 0.5$

FIG. 16: Approximate boundaries between distinct solution regimes for the case with (a) $\delta = 1$ and (b) $\delta = 0.5$. Regimes are labelled as follows: I whole-layer; IIa localized temperature perturbation; IIb localized velocity; IIab localized temperature and velocity; III segregated.

ACKNOWLEDGMENTS

This work was supported by the Engineering and Physical Sciences Research Council (EPSRC) Centre for Doctoral Training in Fluid Dynamics at the University of Leeds under Grant No. EP/L01615X/1. We are grateful to Wayne Arter, Fulvio Militello and Sven Van Loo for useful discussions. We thank the referees for helpful comments.

---

[1] S. Chandrasekhar, *Hydrodynamic and Hydromagnetic Stability*, 3^{rd} ed. (Dover Publications, Inc., 1981).
[2] F. M. Richter and C. E. Johnson, J. Geophys. Res. **79**, 1635 (1974).
[3] F. H. Busse, Phys. Earth Planet. Inter. **24**, 320 (1981).
[4] N. E. Hurlburt, J. Toomre, and J. M. Massaguer, Astrophys. J. **311**, 563 (1986).
[5] A. T. Prakash and J. N. Koster, Int. J. Multiphase Flow **20**, 383 (1994).
[6] S. Rasenat, F. H. Busse, and I. Rehberg, J. Fluid Mech. **199**, 519 (1989).
[7] S. V. Diwakar, S. Tiwari, S. K. Das, and T. Sundararajan, J. Fluid Mech. **754**, 415 (2014).
[8] M. R. E. Proctor and C. A. Jones, J. Fluid Mech. **188**, 301 (1988).
[9] J. Ongena, R. Koch, R. Wolf, and H. Zohm, Nat. Phys. **12**, 398 (2016).
[10] S. I. Krasheninnikov, D. A. D'Ippolito, and J. R. Myra, J. Plasma Phys. **74**, 679 (2008).
[11] D. A. D'Ippolito, J. R. Myra, and S. J. Zweben, Phys. Plasmas **18**, 060501 (2011).
[12] S. I. Braginskii, Rev. Plasma Phys **1**, 205 (1965).
[13] M. Berning and K. Spatschek, Phys. Rev. E **62**, 1162 (2000).
[14] P. Ghendrih, Y. Sarazin, G. Attuel, S. Benkadda, P. Beyer, G. Falchetto, C. Figarella, X. Garbet, V. Grandgirard, and M. Ottaviani, Nucl. Fusion **43**, 1013 (2003).
[15] O. E. Garcia, N. H. Bian, J. V. Paulsen, S. Benkadda, and K. Rypdal, Plasma Phys. Controlled Fusion **45**, 919 (2003).
[16] O. E. Garcia and N. H. Bian, Phys. Rev. E **68**, 047301 (2003).
[17] O. E. Garcia, N. H. Bian, V. Naulin, A. H. Nielsen, and J. J. Rasmussen, Phys. Scr. **2006**, 104 (2006).
[18] N. Bian, S. Benkadda, J. V. Paulsen, and O. E. Garcia, Phys. Plasmas **10**, 671 (2003).
[19] O. E. Garcia, N. H. Bian, V. Naulin, A. H. Nielsen, and J. J. Rasmussen, Phys. Plasmas **12**, 090701 (2005).
[20] O. E. Garcia, N. H. Bian, and W. Fundamenski, Phys. Plasmas **13**, 082309 (2006).
[21] A. Y. Aydemir, Phys. Plasmas **12**, 062503 (2005).
[22] F. Wilczynski, D. W. Hughes, S. Van Loo, W. Arter, and F. Militello, Phys. Plasmas **26**, 022510 (2019).
[23] O. E. Garcia, V. Naulin, A. H. Nielsen, and J. J. Rasmussen, Phys. Plasmas **12**, 062309 (2005).
[24] O. E. Garcia, J. Horacek, R. A. Pitts, A. H. Nielsen, W. Fundamenski, J. P. Graves, V. Naulin, and J. J. Rasmussen, Plasma Phys. Controlled Fusion **48**, L1 (2005).
[25] W. Fundamenski, O. E. Garcia, V. Naulin, R. A. Pitts, A. H. Nielsen, J. J. Rasmussen, J. Horacek, J. P. Graves, *et al.*, Nucl. Fusion **47**, 417 (2007).
[26] F. Militello, W. Fundamenski, V. Naulin, and A. H. Nielsen, Plasma Phys. Controlled Fusion **54**, 095011 (2012).
[27] F. Militello, P. Tamain, W. Fundamenski, A. Kirk, V. Naulin, A. H. Nielsen, *et al.*, Plasma Phys. Controlled Fusion **55**, 025005 (2013).
[28] J. R. Myra, W. M. Davis, D. A. D'Ippolito, B. LaBombard, D. A. Russell, J. L. Terry, and S. J. Zweben, Nucl. Fusion **53**, 073013 (2013).
[29] A. H. Nielsen, J. J. Rasmussen, J. Madsen, G. Xu, V. Naulin, J. M. B. Olsen, M. Løiten, S. Hansen, N. Yan, L. Tophøj, *et al.*, Plasma Phys. Controlled Fusion **59**, 025012 (2016).
[30] M. Le Bars and A. Davaille, J. Fluid Mech. **471**, 339 (2002).
[31] D. A. Nield, J. Fluid Mech. **32**, 393 (1968).
[32] A. Pellew and R. V. Southwell, Proc. R. Soc. Lond. A **176**, 312 (1940).